Effect of random antiferromagnetic exchange on the spin waves in a three-dimensional Heisenberg ferromagnet

S. Hameed[1,*] Z. Wang[1,†] D. M. Gautreau,[1,2] J. Joe,[1] K. P. Olson[2,‡] S. Chi[3] P. M. Gehring[4] T. Hong,[3] D. M. Pajerowski,[3] T. J. Williams[3] Z. Xu,[4] M. Matsuda[3] T. Birol,[2] R. M. Fernandes,[1] and M. Greven[1,§]

[1]*School of Physics and Astronomy, University of Minnesota, Minneapolis, Minnesota 55455, USA*

[2]*Chemical Engineering and Materials Science, University of Minnesota, Minneapolis, Minnesota 55455, USA*

[3]*Neutron Scattering Division, Oak Ridge National Laboratory, Oak Ridge, Tennessee 37831, USA*

[4]*NIST Center for Neutron Research, National Institute of Standards and Technology, Gaithersburg, Maryland 20899, USA*

(Received 5 May 2023; accepted 18 September 2023; published 5 October 2023)

Neutron scattering is used to study spin waves in the three-dimensional Heisenberg ferromagnet $YTiO_3$, with spin-spin exchange disorder introduced via La substitution at the Y site. No significant changes are observed in the spin-wave dispersion up to a La concentration of 20%. However, a strong broadening of the spectrum is found, indicative of shortened spin-wave lifetimes. Density-functional theory calculations predict minimal changes in exchange constants as a result of average structural changes due to La substitution, in agreement with the data. The absence of significant changes in the spin-wave dispersion, the considerable lifetime effect, and the reduced ordered magnetic moment previously observed in the La-substituted system are qualitatively captured by an isotropic, nearest-neighbor, three-dimensional Heisenberg ferromagnet model with random antiferromagnetic exchange. We therefore establish $Y_{1-x}La_xTiO_3$ as a model system for the study of antiferromagnetic spin-exchange disorder in a three-dimensional Heisenberg ferromagnet.

DOI: 10.1103/PhysRevB.108.134406

I. INTRODUCTION

Understanding how disorder affects magnetic ground states is the subject of considerable research, not only due to fundamental scientific interest [1,2], but also because of its potential to advance technologies such as spintronics [3] and magnonics [4]. Arguably the most powerful probe of magnetism is neutron scattering, which enables comprehensive measurements of magnetic order and excitations, and therefore provides pivotal information regarding the spin Hamiltonian that governs a system [5].

The effects of nonmagnetic site dilution in magnetic materials have been well studied theoretically and experimentally (e.g., Refs. [2,6–10]). A prominent example is site dilution in two-dimensional Heisenberg antiferromagnets [9]. Other examples include studies of dilute ferromagnetic (FM) and antiferromagentic (AFM) transition metal fluorides [6–8]. Spin-exchange disorder in the form of intermixed AFM and FM interactions has also been studied theoretically, in the context of spin glasses [11]. The relevant models typically consider a Gaussian distribution of spin exchange, spanning both FM and AFM interactions, but centered around a FM exchange [11]. Such models allow only for FM and spin-glass ground states. The case of a binary distribution of FM and AFM interactions, which allows for both FM and AFM ground states, has also been explored theoretically to some extent [12–14]. However, to the best of our knowledge, measurements of spin waves in experimental realizations of such a spin system with a binary distribution of exchange constants are lacking.

The rare-earth titanates $RTiO_3$ (R being a rare-earth ion) provide a unique platform with which to study the effects of such a binary spin-exchange distribution in a three-dimensional (3D) system. These perovskites are Mott insulators, with a spin-$\frac{1}{2}$ $3d^1$ electronic configuration. They feature a $GdFeO_3$-type distorted structure, with a Ti-O-Ti bond angle that is less than 180°. The nature of the magnetic ground state depends on the R ionic radius, and hence the Ti-O-Ti bond angle. Materials with smaller R ionic radii (i.e., smaller Ti-O-Ti bond angles) exhibit FM ground states (e.g., Y, Gd, Dy), whereas materials with larger R ionic radii (i.e., larger Ti-O-Ti bond angles) exhibit AFM ground states (e.g., La, Sm, Nd) [15]. Mixing different R ions therefore enables the exploration of the effects of admixing FM and AFM spin exchanges in a 3D system [16]. Spin-wave spectra in FM $YTiO_3$ and AFM $LaTiO_3$ were measured previously and shown to be in good agreement with a nearly isotropic 3D Heisenberg FM and AFM model, respectively [17,18]. Furthermore, unlike most other $RTiO_3$ systems, Y^{3+} and La^{3+} lack a magnetic moment, which offers a distinct advantage: The system's magnetic properties stem solely from the Ti^{3+} ions.

In this paper, we study spin waves in the Mott-insulating spin-$\frac{1}{2}$ 3D Heisenberg FM $YTiO_3$, with spin-exchange

*Present address: Max Planck Institute for Solid State Research, Heisenbergstraße 1, 70569 Stuttgart, Germany; Corresponding author: s.hameed@fkf.mpg.de

†Present address: Center for Correlated Matter and School of Physics, Zhejiang University, Hangzhou 310058, China.

‡Present address: Department of Materials Science and Engineering, Northwestern University, Evanston, Illinois 60201, USA.

§Corresponding author: greven@umn.edu

disorder induced via substitution of La at the Y site. We present data up to a La substitution level of $x = 0.22$. We find minimal changes in the spin-wave dispersion, whereas a strong broadening of the spectrum is observed with increasing La substitution. Complementary density-functional theory (DFT) calculations reveal that the average structural changes induced by moderate La substitution are expected to cause only a modest decrease in spin-exchange parameters, in agreement with the data. Spin-wave calculations based on a nearest-neighbor, isotropic Heisenberg FM model with added random AFM spin exchange reveal a shortened spin-wave lifetime, a reduced FM ordered moment, and subtle changes in the spin-wave dispersion with increasing disorder, in good qualitative agreement with the experimental results. $Y_{1-x}La_xTiO_3$ is therefore a model system for the study of AFM spin-exchange disorder effects in a 3D Heisenberg ferromagnet.

II. EXPERIMENTAL METHODS

Single crystals of $Y_{1-x}La_xTiO_3$ were melt grown with the optical floating-zone technique and well characterized postgrowth, as described elsewhere [20]. Triple-axis neutron spectroscopy was performed with the HB-1 and HB-3 thermal-neutron triple-axis spectrometers and the CG-4C cold-neutron triple axis spectrometer at the High Flux Isotope Reactor, located at Oak Ridge National Laboratory, and with the BT-7 thermal-neutron triple-axis spectrometer, located at the NIST Center for Neutron Research. We studied $x = 0$ and $x = 0.10$ single crystals with masses in the 3–4 g range, and an $x = 0.20$ sample composed of 20 coaligned crystals with a total mass of ∼12 g. The larger sample mass for $x = 0.20$ was needed to detect the weaker signal due to the reduced ordered magnetic moment and strongly damped spin waves. Limited data were also collected on $x = 0.15$ and $x = 0.22$ single crystals, with masses of ∼1.5 g each, and a ∼1.5 g, $x = 0.30$ sample that consists of eleven coaligned crystals. The rocking curves for all samples can be found in the Supplemental Material [19]. The detailed procedure adopted to ensure chemical homogeneity of the samples can be found in Ref. [20]. The fixed final energies of the scattered neutrons were 14.7 or 30.5 meV for the thermal-neutron triple-axis measurements, and 4.5 meV for the cold-neutron triple-axis measurements. We used collimations of 48′-80′-sample-80′-120′ at HB-1 and HB-3, open-80′-sample-80′-120′ at BT-7, and open-open-sample-80′-open at CG-4C. Pyrolytic graphite filters were used at HB-1, HB-3 and BT-7, and a cooled Be filter was used at CG-4C, after the sample, to eliminate higher-order neutrons. A ^{4}He cryostat and a closed-cycle refrigerator were used to reach temperatures down to 1.5 and 4 K, respectively. The samples were mounted in the $(0KL)$ scattering plane, and the spin-wave excitations were characterized using energy and momentum scans. Each scan was performed twice: at a temperature well below the respective magnetic transition temperatures (1.5–4 K), and at a temperature well above the magnetic transition temperatures (15–40 K).

III. EXPERIMENTAL RESULTS

Figure 1 shows representative energy scans measured at $(001)_o$ for $x = 0$, 0.10, 0.20, and 0.22. Here, the subscript "o" refers to the orthorhombic reciprocal space notation, which we use throughout this paper. The data obtained in the paramagnetic state were subtracted from the low-temperature data in order to better isolate the magnetic contribution to the inelastic signal in the magnetically ordered state. Clear spin-wave signals are observed for all samples. A strong decrease in intensity is observed with increasing La substitution.

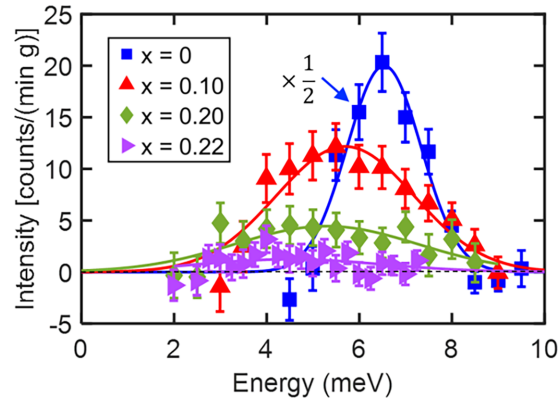

FIG. 1. Representative energy scans at $(0, 0, 1)_o$ (with high-temperature data subtracted) for $x = 0$, 0.10, 0.20, and 0.22, along with respective Gaussian fits. The data for $x = 0$ are scaled down by a factor of 2. See Supplemental Material [19] for additional energy and momentum scans. The error bars correspond to one standard deviation.

At nonzero La concentrations, the signal-to-background ratio was not high enough to accurately extract intrinsic spin-wave lifetimes from a deconvolution with the instrument resolution (see Supplemental Material [19]). Therefore, fits of the net (high-temperature data subtracted) data to a simple Gaussian profile were carried out in all cases. Examples of resultant fits are shown as solid lines in Fig. 1 and in Supplemental Material [19]. The peak positions thus obtained are used to determine the spin-wave dispersion, as shown in Fig. 2(a). The spin-wave spectrum for $YTiO_3$ is in good agreement with prior work [17].

For $YTiO_3$, we found the energy scans to be nearly resolution limited, indicative of very long spin-wave lifetimes. Figures 2(b)–2(d) display color maps of the spin-wave intensities extracted from Gaussian fits to the energy scans for various La substitution levels. We clearly observe that the spin waves broaden in energy with increasing La substitution, a result that is indicative of shortened lifetimes.

IV. COMPARISON TO THEORETICAL CALCULATIONS

In order to shed light on the behavior of the spin-wave spectrum with increasing x, we perform DFT calculations that assume that the main effect of La substitution is to induce structural changes in $Y_{1-x}La_xTiO_3$. Thus, we approximate the crystal structure of $Y_{1-x}La_xTiO_3$ by interpolating between the $YTiO_3$ and $LaTiO_3$ structures. In particular, for a given value of x, the lattice parameters and internal coordinates of $Y_{1-x}La_xTiO_3$ are obtained by linearly interpolating those for bulk $YTiO_3$ and $LaTiO_3$ crystal structures. Such an interpolation is valid given the fact that the unit cell volume increases linearly with x [21,22]. Taking 21 equally spaced

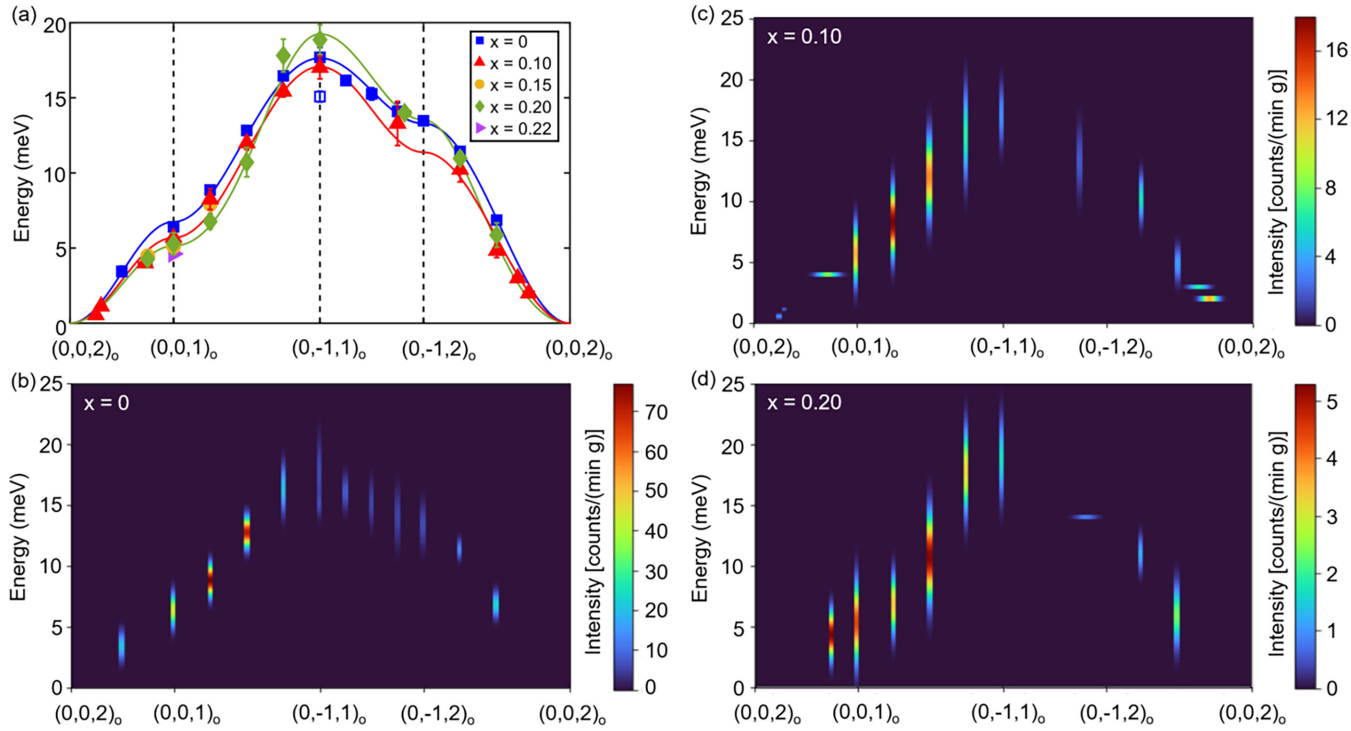

FIG. 2. (a) Spin-wave peak energies at low temperature. For $x = 0$, two peaks were resolved at $(0, -1, 1)_o$, likely as a result of a coupling with an optical phonon branch [17]. The open blue square indicates the second peak. The lines are guides to the eye. The error bars correspond to those obtained from the fits. [(b)–(d)] Spin-wave intensities at low temperature for (b) $x = 0$, (c) $x = 0.10$, and (d) $x = 0.20$, obtained from Gaussian fits to energy scans, as described in the text. The data elongated along the horizontal direction were obtained from momentum scans. The low-energy data at $(0, 0, 1.7)_o$ and $(0, 0, 1.75)_o$ for $x = 0.10$ have a small width in energy as these were taken with a higher energy resolution at a cold-neutron triple-axis spectrometer. The intensities for these were multiplied by a factor of five for better visibility in the color map. The data for $x = 0$ and $x = 0.20$ and the data at $(0, 0, 1.7)_o$ and $(0, 0, 1.75)_o$ for $x = 0.10$ were obtained at 1.5 K. The remaining data were obtained at 4 K.

values of x between $x = 0$ and $x = 1$, we obtain a series of interpolated structures. In each structure, we calculate the energy of 16 collinear spin configurations from first principles (see Supplemental Material [19] for details). These energies are then fit to a nearest-neighbor Heisenberg model to obtain the nearest-neighbor exchange parameters J_{xy} and J_z (see the inset to Fig. 3) as a function of La concentration x. In all calculations, Y is used as the rare-earth ion. This assumption is valid if the effect of La substitution is largely steric in nature. The results are presented in Fig. 3, where we show how J_{xy} and J_z vary with La concentration. Clearly, up to $x = 0.20$, only a modest decrease ($\sim$10%) in $|J_{xy}|$ and $|J_z|$ is expected, consistent with the minimal changes observed in the spin-wave energy scale with increasing La substitution.

In these DFT calculations, we considered only the average structural changes induced by La substitution. Such changes are not expected to drive the shortened spin-wave lifetimes that we observe in our data. In order to understand this, the effect of disorder resulting from the presence of atoms of differing sizes needs to be considered. Since $LaTiO_3$ is an antiferromagnet, in a simple picture, admixing La at the Y site in FM $YTiO_3$ induces AFM spin exchange into the FM host. For simplicity, and motivated by the fact that the spin-wave spectra for $YTiO_3$ and $LaTiO_3$ agree well with isotropic FM and AFM Heisenberg models, respectively [17,18], we consider an isotropic nearest-neighbor Heisenberg ferromagnet with AFM Heisenberg interactions randomly admixed into it. Specifically, we consider the classical Heisenberg model on

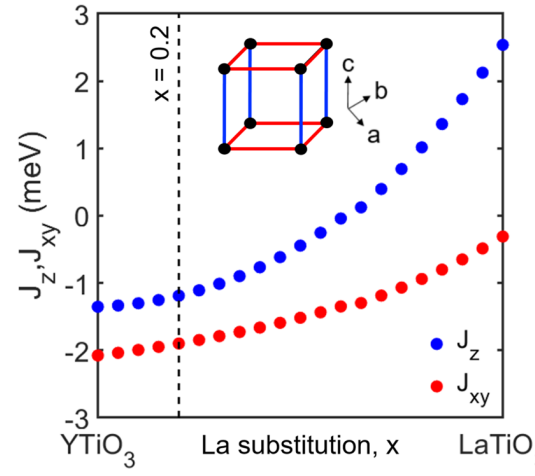

FIG. 3. Effective spin-spin exchange parameters as a function of La substitution determined from DFT. Each La concentration is simulated by interpolating between the known crystal structures for $YTiO_3$ and $LaTiO_3$. J_{xy} and J_z represent spin-exchange parameters between nearest-neighbor Ti ions in the *ab* plane and along the *c* axis, respectively (see inset).

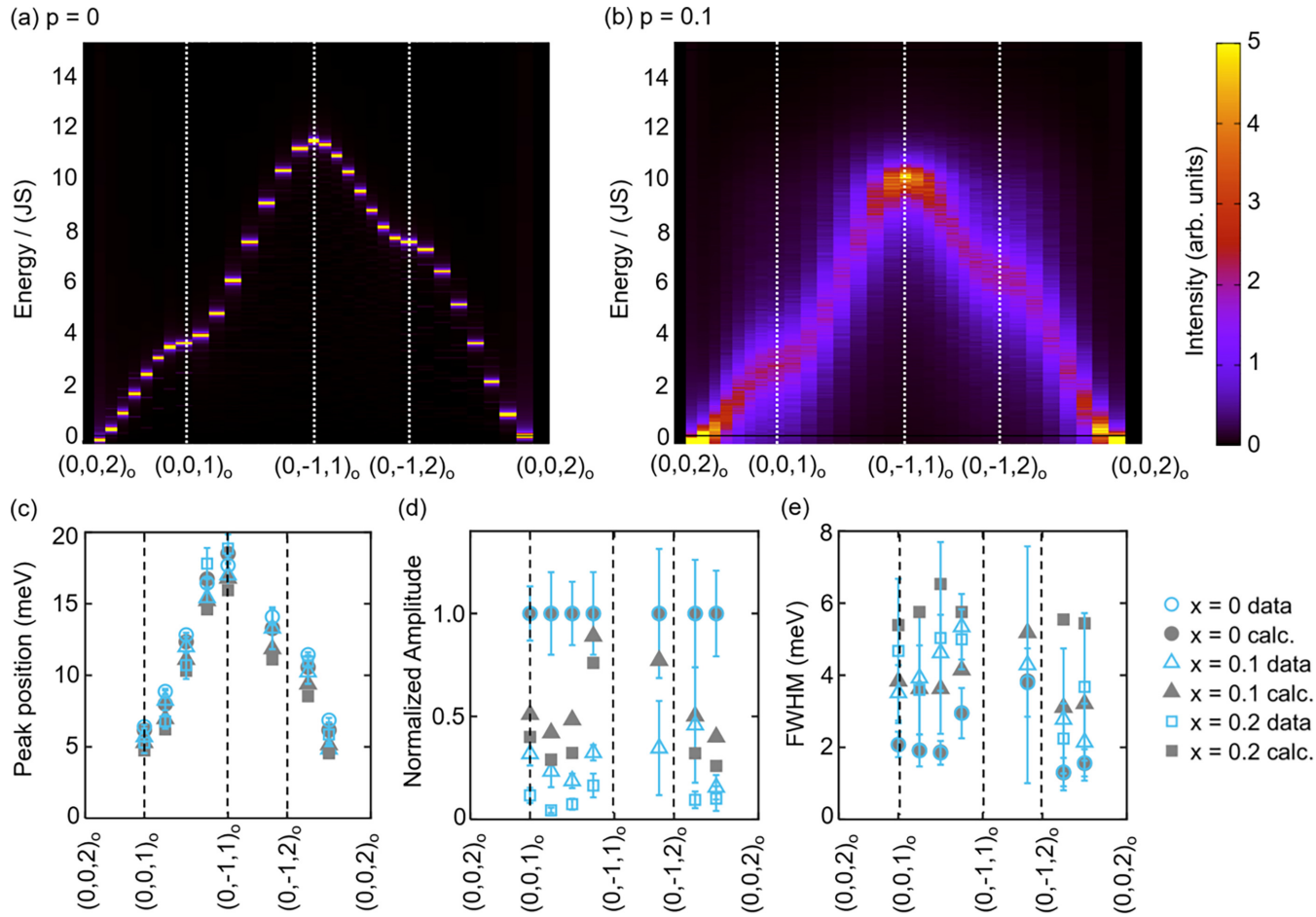

FIG. 4. (a) Calculated dynamic spin structure factor $\mathcal{S}(\boldsymbol{Q}, \omega)$ of model (1) for (a) $p = 0$ and (b) $p = 0.1$, obtained with $L = 16$ and temperature $T = 0.1J$. Here, $S = \frac{1}{2}$. [(c)–(e)] Comparison of the (c) peak positions, (d) amplitude, and (e) full width at half maximum (FWHM) of the calculated and measured spin-wave results at different wave vectors. We set $p = x/2$ for the comparison. The calculated spin-wave spectrum is scaled to best fit (for $p = 0$) the experimental results for $YTiO_3$. At each wave vector, the amplitude is normalized to the $x = p = 0$ value. The theoretical results are convoluted with the instrument resolution to determine the FWHM. Only results at wave vectors for which data are available for multiple La substitution levels are displayed in [(c)–(e)]. The comparison at $(0, -1, 1)_o$ is omitted in (d) and (e) since a coupling to phonons complicates the experimental spin-wave response [17]. For the comparison at $(0, -1, 1)_o$ in (c), we use the higher-energy spin-wave peak obtained for $x = 0$. The error bars in [(c)–(e)] correspond to those obtained from the fits.

an $L \times L \times L$ simple cubic lattice,

$$\mathcal{H} = \sum_{\langle i,j \rangle} J_{ij} \boldsymbol{S}_i \cdot \boldsymbol{S}_j, \tag{1}$$

where J_{ij} is the nearest-neighbor magnetic exchange drawn from a binary distribution: $J_{ij} = -J$ (FM) with probability $1 - p$, and $J_{ij} = 5J$ (AFM) with probability p. The ratio of the FM and AFM exchange constants is chosen to be 1 : 5, to match the ratio of the Heisenberg spin exchanges in $YTiO_3$ ($\sim$3 meV) [17] and $LaTiO_3$ ($\sim$15.5 meV) [18]. The dynamic spin structure factor was calculated on an $L = 16$ cubic lattice using replica exchange Monte Carlo with heat-bath and overrelaxation updates [23–26], followed by the equation-of-motion method [27], and averaged over 50 disorder realizations (see Supplemental Material [19] for details). The calculated spin-wave spectra are displayed in Figs. 4(a) and 4(b) for $p = 0$ and $p = 0.1$, respectively. Note that the spin-wave intensities for $p = 0$ in Fig. 4(a) do not change with $\boldsymbol{Q}$. This is indeed as expected from linear spin-wave theory, where the dynamic spin structure factor has the form $\mathcal{S}(\boldsymbol{Q}, \omega) = 2\pi S \delta(\omega - \omega_{\boldsymbol{Q}})$, $\omega_{\boldsymbol{Q}}$ being the dispersion. This further confirms that our combined Monte Carlo and equation-of-motion approach is valid. A strong broadening in the spin-wave intensity is observed for nonzero p, while the zone-boundary energy remains approximately constant. This is in qualitative agreement with our data. Experimentally, we cannot rule out the possibility that the La ions cluster together. If such clustering were present, one would expect that the local Ti-O-Ti bond angle closely resembles that of $LaTiO_3$ and hence leads to an AFM spin exchange between the neighboring spin-$\frac{1}{2}$ Ti^{3+} ions. However, too much clustering of the La ions is not very likely because La has the same charge as Y and the perovskite structure is rather flexible in accommodating different cations on the R site. If we assume clustering at the level of $4 \times 4 \times 4$ unit cell volume, we can expect one AFM spin-exchange bond for every two La ions. Motivated by this feature, and to make the comparison with experiment more quantitative, we relate p and x according to $p \approx x/2$. Despite the simplicity of the model, it qualitatively

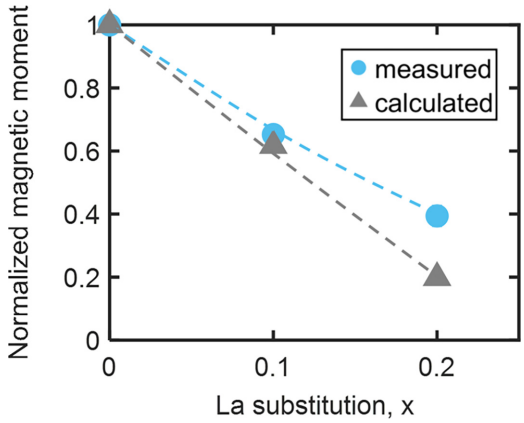

FIG. 5. Calculated FM moment $\sqrt{[\langle m^2\rangle]_{\rm av}}$ obtained for the disordered Heisenberg model with $L = 16$ and $T/J = 0.1$ (the error bars are smaller than the symbol size), compared with prior data for $Y_{1-x}La_xTiO_3$ (from Ref. [28]). We set $p = x/2$ for the comparison. The FM moment values are normalized to the value at $x = p = 0$.

captures the key experimental observations with increasing x: (i) minimal changes in the spin-wave dispersion [Fig. 4(c)]; (ii) a strong decrease of the spin-wave amplitude [Fig. 4(d)]; (iii) a strong reduction in the spin-wave lifetime [Fig. 4(e)]; and (iv) a strong decrease in the FM ordered moment with increasing x (Fig. 5). Although the experimental trends are reasonably captured by our model, there are quantitative deviations. For instance, the experimental spin-wave amplitude falls off more strongly than the calculations [Fig. 4(d)]. The deviation near the zone boundary is particularly severe, most likely due to magnon-phonon crossing [17], which is not considered in our model. A more detailed theoretical description is beyond the scope of this work in light of the experimental constraint of low signal-to-noise ratios even with a large sample mass. Nevertheless, given the good qualitative agreement of the calculations with the data, we can conclude that the magnetic properties of $Y_{1-x}La_xTiO_3$ in the La substitution range up to $x \sim 0.2$ are dominated by effective AFM spin-exchange disorder introduced by the La substitution. In prior theoretical work on FM systems with admixed AFM interactions, it was suggested that local AFM spin waves form [14]. Attempts to find such local modes experimentally at the zone boundary were unsuccessful [19]. However, we cannot rule out the possibility that such spin waves are too weak in amplitude to be observable in our measurements.

V. CONCLUSIONS

To summarize, we used neutron scattering to measure spin waves in the 3D Heisenberg ferromagnet $Y_{1-x}La_xTiO_3$. No significant changes are observed in the spin-wave dispersion. In contrast, a strong broadening and weakening of the spin-wave intensity is observed with increasing La concentration. We find good qualitative agreement with calculations for an isotropic nearest-neighbor FM Heisenberg model with randomly admixed AFM spin exchange. We therefore conclude that, at substitution levels up to $x \approx 0.2$, $Y_{1-x}La_xTiO_3$ is a model 3D Heisenberg ferromagnet with AFM spin-exchange disorder.

ACKNOWLEDGMENTS

The work at University of Minnesota was funded by the Department of Energy through the University of Minnesota Center for Quantum Materials, under Grant No. DE-SC0016371. Parts of this work were carried out in the Characterization Facility, University of Minnesota, which receives partial support from the NSF through the MRSEC (Award No. DMR-2011401) and the NNCI (Award No. ECCS-2025124) programs. A portion of this research used resources at the High Flux Isotope Reactor, a DOE Office of Science User Facility operated by the Oak Ridge National Laboratory. We acknowledge the support of the National Institute of Standards and Technology, U.S. Department of Commerce, in providing the neutron research facilities used in this work.

[1] I. Y. Korenblit and E. F. Shender, Chapter 3: Theory of magnetic excitations in disordered systems, in *Spin Waves and Magnetic Excitations*, edited by A. S. Borovik-Romanov and S. K. Sinha, Modern Problems in Condensed Matter Sciences Vol. 22 (Elsevier, Amsterdam, 1988), pp. 109–175.

[2] R. J. Elliott, J. A. Krumhansl, and P. L. Leath, The theory and properties of randomly disordered crystals and related physical systems, Rev. Mod. Phys. **46**, 465 (1974).

[3] A. H. MacDonald, P. Schiffer, and N. Samarth, Ferromagnetic semiconductors: Moving beyond (Ga,Mn)As, Nat. Mater. **4**, 195 (2005).

[4] A. Barman, G. Gubbiotti, S. Ladak, A. O. Adeyeye, M. Krawczyk, J. Gräfe, C. Adelmann, S. Cotofana, A. Naeemi, V. I. Vasyuchka, B. Hillebrands, S. A. Nikitov, H. Yu, D. Grundler, A. V. Sadovnikov, A. A. Grachev, S. E. Sheshukova, J.-Y. Duquesne, M. Marangolo, G. Csaba *et al.*, The 2021 magnonics roadmap, J. Phys.: Condens. Matter **33**, 413001 (2021).

[5] G. Shirane, S. M. Shapiro, and J. M. Tranquada, *Neutron Scattering with a Triple-Axis Spectrometer: Basic Techniques* (Cambridge University Press, Cambridge, UK, 2002).

[6] R. A. Cowley and W. J. L. Buyers, The properties of defects in magnetic insulators, Rev. Mod. Phys. **44**, 406 (1972).

[7] V. Wagner and U. Krey, Spin wave excitations in the dilute two-dimensional ferromagnet $K_2Cu_{1-x}Zn_xF_4$, Z Phys. B **30**, 367 (1978).

[8] T. Nakayama, K. Yakubo, and R. L. Orbach, Dynamical properties of fractal networks: Scaling, numerical simulations, and physical realizations, Rev. Mod. Phys. **66**, 381 (1994).

[9] O. P. Vajk, P. K. Mang, M. Greven, P. M. Gehring, and J. W. Lynn, Quantum impurities in the two-dimensional spin one-half Heisenberg antiferromagnet, Science **295**, 1691 (2002).

[10] R. M. Fernandes and J. Schmalian, Complex critical exponents for percolation transitions in Josephson-junction arrays, antiferromagnets, and interacting bosons, Phys. Rev. Lett. **106**, 067004 (2011).

[11] K. Binder and A. P. Young, Spin glasses: Experimental facts, theoretical concepts, and open questions, Rev. Mod. Phys. **58**, 801 (1986).

[12] M. V. Feigel'man and A. M. Tsvelik, Localized degrees of freedom in a ferromagnet with resonant impurities, Zh. Eksp. Teor. Fiz. **76**, 2249 (1979) [Sov. Phys. JETP **49**, 1136 (1979)].

[13] M. V. Medvedev, Spin waves in a uniaxial ferromagnet with random exchange bonds of different signs, Phys. Status Solidi B **88**, 117 (1978).

[14] S. L. Ginzburg, Contribution to the theory of ferromagnets with admixture of antiferromagnetic bonds, Zh. Eksp. Teor. Fiz. **76**, 2330 (1979) [Sov. Phys. JETP **49**, 1127 (1979)].

[15] M. Mochizuki and M. Imada, Orbital physics in the perovskite Ti oxides, New J. Phys. **6**, 154 (2004).

[16] Z. Wang, D. Gautreau, T. Birol, and R. M. Fernandes, Strain-tunable metamagnetic critical endpoint in Mott insulating rare-earth titanates, Phys. Rev. B **105**, 144404 (2022).

[17] C. Ulrich, G. Khaliullin, S. Okamoto, M. Reehuis, A. Ivanov, H. He, Y. Taguchi, Y. Tokura, and B. Keimer, Magnetic order and dynamics in an orbitally degenerate ferromagnetic insulator, Phys. Rev. Lett. **89**, 167202 (2002).

[18] B. Keimer, D. Casa, A. Ivanov, J. W. Lynn, M. v. Zimmermann, J. P. Hill, D. Gibbs, Y. Taguchi, and Y. Tokura, Spin dynamics and orbital state in $LaTiO_3$, Phys. Rev. Lett. **85**, 3946 (2000).

[19] See Supplemental Material at http://link.aps.org/supplemental/10.1103/PhysRevB.108.134406 for rocking curves for all samples, raw spin-wave data at all La concentrations, raw energy scans showing the absence of antiferromagnetic spin waves in $x = 0.30$, a comparison between $YTiO_3$ spin-wave spectra obtained via instrument resolution deconvolution and simple Gaussian fitting, details regarding the DFT calculations, and details regarding the Monte Carlo simulations (which contains Refs. [29–35]).

[20] S. Hameed, J. Joe, L. R. Thoutam, J. Garcia-Barriocanal, B. Yu, G. Yu, S. Chi, T. Hong, T. J. Williams, J. W. Freeland, P. M. Gehring, Z. Xu, M. Matsuda, B. Jalan, and M. Greven, Growth and characterization of large (Y,La)TiO_3 and (Y,Ca)TiO_3 single crystals, Phys. Rev. Mater. **5**, 125003 (2021).

[21] H. D. Zhou and J. B. Goodenough, Evidence for two electronic phases in $Y_{1-x}La_xTiO_3$ from thermoelectric and magnetic susceptibility measurements, Phys. Rev. B **71**, 184431 (2005).

[22] J. P. Goral, J. E. Greedan, and D. A. MacLean, Magnetic behavior in the series $La_xY_{1-x}TiO_3$, J. Solid State Chem. **43**, 244 (1982).

[23] K. Hukushima and K. Nemoto, Exchange Monte Carlo method and application to spin glass simulations, J. Phys. Soc. Jpn. **65**, 1604 (1996).

[24] Y. Miyatake, M. Yamamoto, J. J. Kim, M. Toyonaga, and O. Nagai, On the implementation of the heat bath algorithms for Monte Carlo simulations of classical Heisenberg spin systems, J. Phys. C: Solid State Phys. **19**, 2539 (1986).

[25] M. Creutz, Overrelaxation and Monte Carlo simulation, Phys. Rev. D **36**, 515 (1987).

[26] F. R. Brown and T. J. Woch, Overrelaxed heat-bath and Metropolis algorithms for accelerating pure gauge Monte Carlo calculations, Phys. Rev. Lett. **58**, 2394 (1987).

[27] R. Alben and M. F. Thorpe, Spin waves in a random two-dimensional antiferromagnet, J. Phys. C: Solid State Phys. **8**, L275 (1975).

[28] S. Hameed, S. El-Khatib, K. P. Olson, B. Yu, T. J. Williams, T. Hong, Q. Sheng, K. Yamakawa, J. Zang, Y. J. Uemura, G. Q. Zhao, C. Q. Jin, L. Fu, Y. Gu, F. Ning, Y. Cai, K. M. Kojima, J. W. Freeland, M. Matsuda, C. Leighton *et al.*, Nature of the ferromagnetic-antiferromagnetic transition in $Y_{1-x}La_xTiO_3$, Phys. Rev. B **104**, 024410 (2021).

[29] G. Kresse and J. Hafner, *Ab initio* molecular dynamics for liquid metals, Phys. Rev. B **47**, 558 (1993).

[30] G. Kresse and J. Furthmüller, Efficiency of *ab-initio* total energy calculations for metals and semiconductors using a plane-wave basis set, Comput. Mater. Sci. **6**, 15 (1996).

[31] G. Kresse and J. Furthmüller, Efficient iterative schemes for *ab initio* total-energy calculations using a plane-wave basis set, Phys. Rev. B **54**, 11169 (1996).

[32] J. P. Perdew, A. Ruzsinszky, G. I. Csonka, O. A. Vydrov, G. E. Scuseria, L. A. Constantin, X. Zhou, and K. Burke, Restoring the density-gradient expansion for exchange in solids and surfaces, Phys. Rev. Lett. **100**, 136406 (2008).

[33] S. L. Dudarev, G. A. Botton, S. Y. Savrasov, C. J. Humphreys, and A. P. Sutton, Electron-energy-loss spectra and the structural stability of nickel oxide: An LSDA+U study, Phys. Rev. B **57**, 1505 (1998).

[34] V. I. Anisimov, J. Zaanen, and O. K. Andersen, Band theory and Mott insulators: Hubbard U instead of Stoner I, Phys. Rev. B **44**, 943 (1991).

[35] G. Kotliar, S. Y. Savrasov, K. Haule, V. S. Oudovenko, O. Parcollet, and C. A. Marianetti, Electronic structure calculations with dynamical mean-field theory, Rev. Mod. Phys. **78**, 865 (2006).